

# Large-Scale Hierarchically Structured Conjugated Polymer Assemblies with Enhanced Electrical Conductivity\*\*

Wei Han, Ming He, Myunghwan Byun, Bo Li, and Zhiqun Lin\*

Conjugated polymers have been widely recognized as promising materials, with possible applications in photonics, biosensors, electronics, and solar-energy conversion.<sup>[1]</sup> Of the various conjugated polymers, poly(3-alkylthiophenes) (P3ATs; for example, poly(3-hexylthiophene) (P3HT) and poly(3-butylthiophene) (P3BT)) are among the most heavily studied organic semiconductors. They consist of a rather rigid thienyl backbone with a regular head-to-tail arrangement of pendant alkyl side chains that allow for efficient  $\pi$ - $\pi$  stacking of the conjugated backbones and good solubility, which lead to easy handling in solution, excellent chemical stability, and high field-effect mobility.<sup>[2]</sup> The self-organized chains of P3ATs are greatly influenced by the length of the alkyl side chains, regioregularity, molecular weight, solvent properties, and processing conditions (e.g., spin-coating, dip coating, or drop casting), resulting in variations of the charge carrier mobility in thin-film transistors by several orders of magnitude.<sup>[2,3]</sup> Recent advances in synthesis techniques have made possible the design of functional rod-coil and rod-rod block copolymers with a controlled ratio of two dissimilar blocks.<sup>[4]</sup> Recently, in contrast to P3AT homopolymers, P3AT-based rod-rod diblock copolymers (e.g., poly(3-butylthiophene)-*b*-poly(3-hexylthiophene), P3BHT) have been shown to give a much better balance between the chain flexibility and self-assembly by adjusting the ratio of alkyl side chains (P3BT:P3HT), and have completely different solubilities and  $\pi$ - $\pi$  stacking interactions of the polymer chains from their homopolymer counterparts.<sup>[5]</sup> Importantly, the crystallization of conjugated polymers can be optimized using solvent vapor annealing, thus yielding highly ordered molecular packing of conjugated polymer chains for efficient charge transport.<sup>[6]</sup> The ability to organize conjugated polymers into

hierarchically structured assemblies may enable the development of high-performance electronic devices at low cost.

When a freely evaporating droplet containing nonvolatile solutes (e.g., particles, polymers, DNA) wets the surface and its contact line is pinned, the solutes flow to the drop periphery, yielding the familiar and often stochastic “coffee-ring” patterns rather than uniform deposits. To fully capitalize on evaporation as a simple route to well-ordered structures, control over the evaporation process, including the evaporative flux, solution concentration, and interfacial interaction between the solute and substrate, is of key importance. In this context, a few recent preparative approaches have yielded complex structures and assemblies with unprecedented regularity by allowing the drying droplet to evaporate in a confined geometry,<sup>[7]</sup> including a curve-on-flat geometry<sup>[8]</sup> and cylindrical tube.<sup>[9]</sup> The confined geometry provides a unique environment to control the drying dynamics and flow, which in turn promotes the assembly of materials into highly ordered structures with engineered optical, electronic, optoelectronic, and magnetic properties.<sup>[8a,c,10]</sup> When compared with conventional lithography techniques, these evaporative assembly techniques are simple and cost-effective, offering a lithography- and external-field-free means of organizing nonvolatile materials into ordered microscopic structures.

Herein, we present a facile and robust route to creating hierarchical assemblies of conjugated polymers by subjecting a drying droplet containing conjugated polymers to a geometry consisting of a cylinder on a Si substrate (i.e., cylinder-on-Si geometry; Figure 1a). Two conjugated homopolymers (P3HT and P3BT) and one all-conjugated diblock copolymer (P3BHT) were used in our study. Owing to different interfacial interactions between the conjugated polymers and the substrate, the hierarchical assemblies were composed of a set of highly ordered straight or wavy stripes at the microscopic scale over a large area and fiber-like or nodule-like domains at the nanometer scale within each microscopic stripe. These hierarchically structured conjugated polymers and all-conjugated diblock copolymer exhibited good electrical properties. The crystallinity of the as-prepared assemblies of all-conjugated diblock copolymer was improved following chloroform vapor annealing, resulting in a four times increase in electrical conductivity.

The choice of P3HT, P3BT, and P3BHT (P3BT:P3HT = 2:1; molar ratio) as the nonvolatile solutes was motivated by their promising applications in LEDs, solar cells, and thin-film transistors with high field-effect mobility.<sup>[5a,11]</sup> Herein, newly synthesized diblock copolymers were used as nonvolatile solutes to prepare P3HT, P3BT, and P3BHT toluene solutions (0.15 mg mL<sup>-1</sup>; see Supporting Information). The polymer

[\*] Dr. W. Han, B. Li, Prof. Z. Lin  
School of Materials Science and Engineering  
Georgia Institute of Technology, Atlanta, GA 30332 (USA)  
E-mail: zhiqun.lin@mse.gatech.edu

Dr. M. He  
State Key Laboratory of Molecular Engineering of Polymers  
Department of Macromolecular Science, Fudan University  
Shanghai, 200433 (China)

Dr. M. Byun  
Department of Polymer Science and Engineering  
University of Massachusetts, Amherst, MA 01002 (USA)

[\*\*] We gratefully acknowledge support from the National Science Foundation (NSF CBET-1153660 and CMMI-1153663), Georgia Institute of Technology, and Key Laboratory of Computational Physical Sciences at Fudan University, Shanghai, China.

Supporting information for this article is available on the WWW under <http://dx.doi.org/10.1002/anie.201209632>.

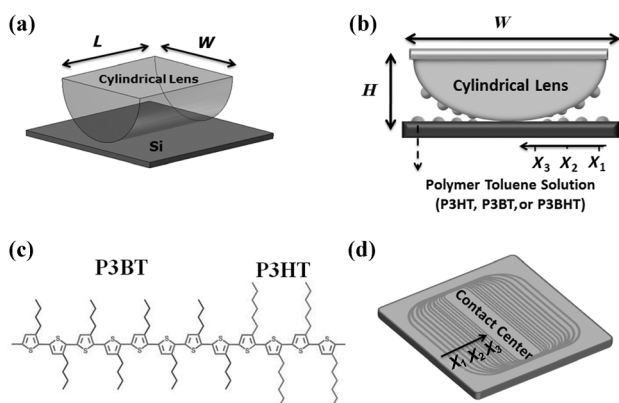


**Figure 1.** a,b) Formation of conjugated polymer stripes. A drop of conjugated polymer toluene solution was confined to a geometry consisting of a cylindrical lens on a flat Si substrate. a) 3D view and b) side view, where  $H$  = height,  $L$  = length, and  $W$  = width of the cylindrical lens.  $X_n$  ( $n = 1-3$ ) is the distance from the deposit to the cylinder/Si contact center. c) Chemical formula of P3BHT diblock copolymer (molar ratio of P3BT/P3HT = 2:1). d) The set of conjugated polymer stripes with a gradient formed by controlled evaporative self-assembly.

toluene solution was trapped in the gap between a cylindrical lens and a Si substrate, which was held in place by capillary force, (Figure 1 a,b), from which toluene was allowed to evaporate only at the capillary edge. The evaporation of toluene triggered the pinning of the three-phase contact line (“stick”), resulting in the deposition of the outermost conjugated polymer stripe (Figure 1 b,d; marked with  $X_1$ , where  $X_1$  is the distance from the first deposit to the cylinder/Si contact center). During this process, the initial contact angle of the meniscus gradually decreased to a critical value, at which the depinning force became larger than the pinning force, causing the contact line to jump to a new position inward (i.e., “slip” toward the cylinder/Si contact center) and arrested to produce a new stripe.<sup>[8d]</sup> The consecutive controlled “stick–slip” cycles of the receding contact line in the cylinder-on-Si geometry yielded a set of stripes with a gradient (Figure 1 d), as a direct consequence of the competition between the linear pinning force and the nonlinear capillary force (i.e., depinning force).<sup>[8d]</sup> The nonlinear depinning force originated from the curved surface topology of the cylindrical lens.<sup>[8d]</sup>

After complete toluene evaporation, the P3HT, P3BT, and P3BHT stripes deposited on the Si substrate were examined with optical microscopy (OM). Figure S1 (in the Supporting Information) shows representative optical micrographs of highly ordered, microscopic stripes of P3HT, P3BT, and P3BHT. The use of the cylinder-on-Si geometry gave stripes over a large area with high regularity. Representative atomic force microscopy (AFM) images taken in three different regions (outermost region,  $X_1 = 4500 \mu\text{m}$ , intermediate region,  $X_2 = 4000 \mu\text{m}$ , and innermost region,  $X_3 = 3500 \mu\text{m}$ ) are shown in Figure 2 and Figures S2–S4. The striped patterns were formed over a large area ( $2X_1 = 9000 \mu\text{m}$  and  $L = 11.0 \text{ mm}$ ), dictated by the volume of the conjugated polymer solution and the width of the cylindrical lens (see Supporting Information). A close inspection of the

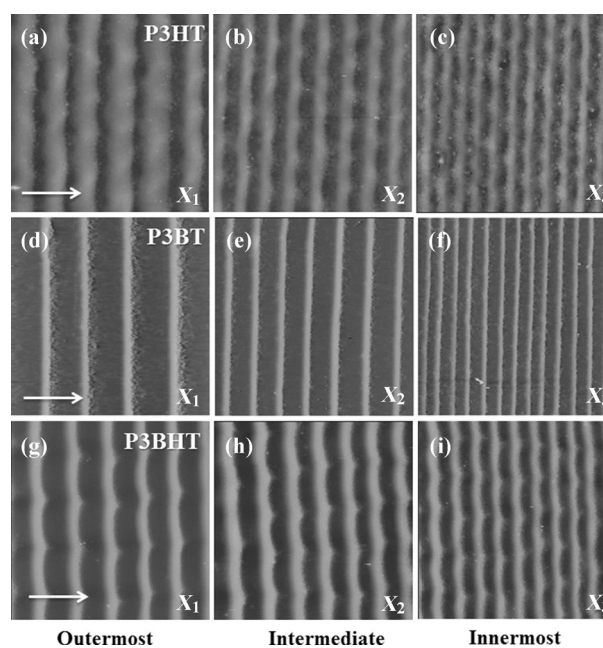


**Figure 2.** Representative AFM height images of conjugated polymer stripes taken in the three different regions ( $X_1$ – $X_3$ ). a–c) P3HT; d–f) P3BT; g–i) P3BHT.  $X_1$  is the outermost region,  $X_2$  is an intermediate region, and  $X_3$  is the innermost region. Image size =  $80 \times 80 \mu\text{m}^2$ . Z range = 400 nm for (a, d, g); 300 nm for (b, e, h); and 200 nm for (c, f, i).

stripes revealed that the width ( $w$ ), height ( $h$ ), and center-to-center distance ( $\lambda_{c,c}$ ) between adjacent stripes progressively decreased with increased proximity to the cylinder/Si contact center (Figure 2), as summarized in Table S1.

Interestingly, the P3BT stripes were straight, while the P3HT and P3BHT stripes clearly displayed fingering instabilities along the stripes (i.e., wavy stripes). Because the solution concentration ( $c = 0.15 \text{ mg mL}^{-1}$ ) and the loading volume of the solution ( $v = 30 \mu\text{L}$ ) were kept the same for all three samples, the difference in the resulting surface patterns was most likely due to different interfacial interactions between the polymer and the Si substrate.<sup>[12]</sup> Increasing the length of the alkyl side chains from butyl to hexyl increased the contact angle of water on conjugated polymer films, suggesting that P3HT was more hydrophobic than P3BT.<sup>[13]</sup> As a result, P3HT and the Si substrate had higher interfacial energy when depositing P3HT on a hydrophilic Si substrate with 2 nm thick native silicon oxide on its surface.<sup>[13]</sup> This unfavorable interfacial interaction between P3HT and Si was responsible for the emergence of the fingering instabilities we observed. Moreover, the P3HT chains did not entangle one another because of their rigid rod-like nature, and the molecular weight (MW) of P3HT was low ( $M_n = 19000 \text{ g mol}^{-1}$ ), thus, P3HT fingers were easily formed (Figure S1 a and Figure 2 a–c).<sup>[8c]</sup> By contrast, the higher MW of P3BT ( $M_n = 22400 \text{ g mol}^{-1}$ ) and lower interfacial energy on the substrate formed straight stripes (Figure S1 b and Figure 2 d–f). For the all-conjugated diblock copolymer P3BHT, fingering instabilities were also seen; this is not surprising owing to the presence of the P3HT blocks in P3BHT (Figure S1 c and Figure 2 g–i). This observation was also

seen with the drying-mediated self-assembly of polystyrene-*block*-poly(methyl methacrylate) (PS-*b*-PMMA),<sup>[12]</sup> where the PS block had an unfavorable interfacial interaction with Si while PMMA had a favorable interaction.<sup>[12]</sup>

Considerable improvements on the crystallinity of conjugated polymers have been made, including the application of thermal annealing<sup>[14]</sup> and solvent vapor annealing,<sup>[15]</sup> to achieve optimized molecular organization and thus enhanced electrical conductivity. Solvent vapor annealing is one of the most robust methods to promote morphological rearrangement of nanodomains within microscopic structures.<sup>[7,10]</sup> In our study, the as-prepared P3BT, P3HT, and P3BHT stripes were exposed to chloroform vapor for 12 hours. Chloroform vapor annealing was chosen because of the good solubility of P3AT-based conjugated polymers in chloroform; they tend to form more thermodynamically favorable crystal structures, composed of edge-on side chains and a parallel orientation of  $\pi$ - $\pi$  stacking planes with respect to the substrate.<sup>[16]</sup>

After chloroform vapor annealing, no obvious topological changes to the P3BT, P3HT, and P3BHT stripes were observed (Figure S5). However, AFM images of the stripes revealed that nanodomains within the microscopic stripes changed upon chloroform vapor annealing (Figure 3a and Figure S6). Because P3AT crystals have well-defined shapes (owing to their rigid thienyl rings), bright features observed in the AFM images are assumed to be crystals.<sup>[6b]</sup> P3HT showed typical nodule-like nanodomains within the stripe after complete evaporation of toluene (top left, Figure 3a),<sup>[6b]</sup> and no obvious changes in the crystal morphology and domain size after subsequent chloroform vapor annealing (top right, Figure 3a), signifying that the crystallinity was not significantly altered by the solvent vapor treatment. Similar crystal morphology was observed in the as-prepared P3BT stripes (center left, Figure 3a), but the size of the P3BT crystals decreased with the emergence of large empty spaces in the AFM phase image after vapor annealing (center right, Figure 3a), indicating a reduction in P3BT crystallinity within the stripe. In contrast with P3HT and P3BT, P3BHT clearly exhibited nanofiber-like morphology within the stripe prior to the vapor annealing (bottom left, Figure 3a). Strikingly, the nanofibers grew into nodules when exposed to the chloroform vapor, suggesting an increase in crystallinity. The nodule-like morphology commonly seen in high MW P3HT gave a high-performance thin-film transistor whereas the nanofibrillar structures often seen in low MW P3HT had four orders-of-magnitude lower charge carrier mobility.<sup>[6b]</sup> Enhanced electrical conductivity of P3BHT after chloroform vapor annealing may thus be a result of the morphological transformation from nanofibers to nodules, because the nodules could connect the ordered regions, offering more pathways for charge transport between crystalline domains.<sup>[3b]</sup>

To further characterize the molecular organization and crystallinity of P3HT, P3BT and P3BHT before and after the solvent vapor annealing, the stripe samples were characterized by XRD following AFM imaging (Figure 3b). The XRD profiles suggested that P3HT, P3BT, and P3BHT stripes had the typical edge-on orientation in which the thienyl backbone was aligned parallel to the Si substrate with the alkyl side chains perpendicular, as we had previously reported.<sup>[17]</sup> The

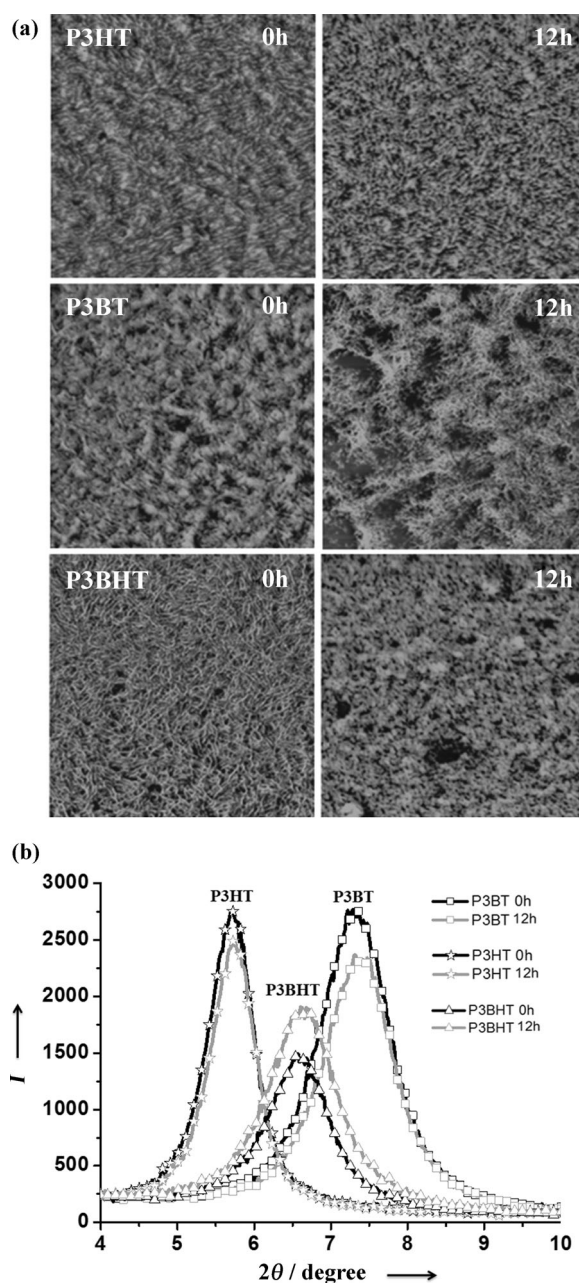


**Figure 3.** a) Representative AFM phase images within the microscopic conjugated polymer stripes before (left) and after (right) the chloroform vapor annealing for 12 hours. Top: P3HT; middle: P3BT; bottom: P3BHT. Image size =  $1.5 \times 1.5 \mu\text{m}^2$ . b) XRD patterns of conjugated polymer stripes (the [100] peak) before (black line) and after (gray line) chloroform vapor annealing for 12 hours.

XRD patterns were measured on the same samples before and after the vapor annealing, so the intensity of the [100] peak (showing the interchain interaction of the alkyl side chains<sup>[4]</sup>) was proportional to the number of polymer crystals per unit volume in the sample, which can be used to compare the change in crystallinity.<sup>[18]</sup> The intensity of the [100] peak of vapor-annealed P3BT decreased, which correlated well with the decrease in crystal domains seen in the AFM phase image (Figure 3a), suggesting that the chloroform vapor tended to dissolve the P3BT chains rather than promoting crystalliza-

tion. By contrast, the [100] peak of P3BHT increased after vapor annealing. This indicates increased crystallinity, in addition to the morphological change from nanofibers to nodule-like aggregates (Figure 3a). Obviously, chloroform vapor annealing promoted rearrangement of the P3BHT nanodomains within the microscopic stripe. The change in the [100] peak intensity of P3HT was rather weak, consistent with no discernible change in the crystal morphology, as shown by AFM (Figure 3a).

It is of practical interest to explore the increased crystallinity of conjugated polymer stripes produced by controlled evaporative self-assembly in the cylinder-on-Si geometry. Current measurements were performed at a constant applied voltage on the stripes formed on the Si substrate before and after vapor annealing (Figure 4). To facilitate the

was nearly unchanged (Figure S5), the large increase in conductivity can primarily be attributed to its improved crystallinity from the vapor annealing. In stark contrast to P3BHT, the conductivity of P3HT stripes was slightly increased and P3BT stripes was markedly decreased, corresponding to the nearly unchanged crystallinity of P3HT and the decreased crystallinity of P3BT, as shown by the AFM and XRD measurements. A slight decrease in the [100] peak of P3HT by XRD (Figure 3b) and slight increase of current in the P3HT stripes (Figure 4b) can be rationalized as follows: the partial dissolution of P3HT by the chloroform vapor may cause a slight decrease in crystallinity (Figure 3b), but the vapor annealing could also improve the connectivity between the P3HT crystals, which in turn enhances conductivity. Consequently, the current of P3HT stripes was slightly increased.<sup>[20]</sup>

In summary, we demonstrated a viable, scalable route to hierarchically structured assemblies composed of microscopic highly ordered stripes with a gradient and nanofibers or nodules within the stripes by evaporating a conjugated P3BT, P3BHT, or all-conjugated P3BHT diblock copolymer toluene solution in an axially symmetric cylinder-on-Si geometry. The morphological rearrangement of nanodomains within the stripes was achieved by the subsequent solvent vapor annealing. In particular, vapor annealing greatly improved the crystallinity of P3BHT, giving a fourfold increase in electrical conductivity. This facile deposition technique based on controlled evaporative self-assembly may serve as a powerful strategy for creating highly structured, multifunctional materials and devices for applications in optoelectronics, photonics, and biosensors.

Received: December 1, 2012

Published online: January 25, 2013

**Keywords:** block copolymers · conjugated polymers · evaporative self-assembly · electrical conductivity · self-assembly

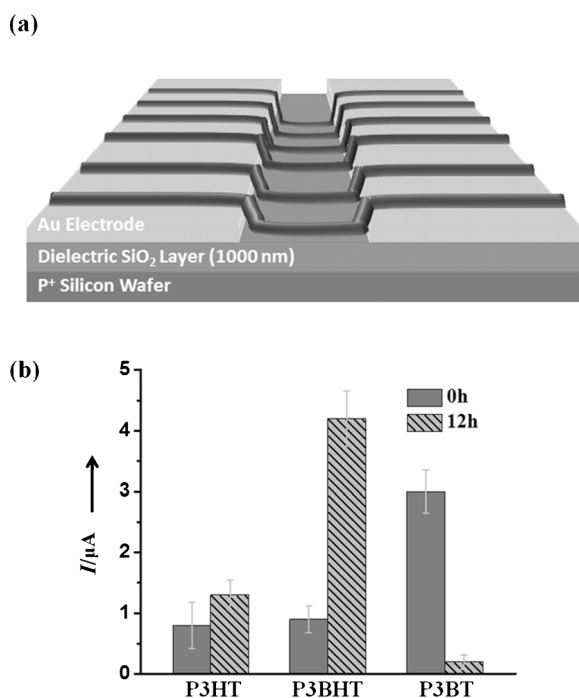


**Figure 4.** Electrical conductivity of P3HT, P3BT, and P3BHT before and after the vapor annealing. a) Scheme of the electrical conductivity measurement; stripes were formed directly on Au electrodes predeposited on the Si substrate. b) Current measurements for P3BT, P3BHT, and P3HT stripes before (dark gray) and after (striped gray) the chloroform vapor annealing for 12 hours measured at an applied voltage of 10 V.

conductivity measurement, the stripes were formed directly (using controlled evaporative self-assembly) on a Si substrate that was predeposited with two Au electrodes separated by a 50 µm gap (Figure 4a). All as-prepared stripe samples exhibited good electrical conductivity (Figure 4b), especially the P3BT sample because of its short butyl side chains and thus relatively high crystallinity.<sup>[6a,19]</sup> The conductivity of the P3BHT stripes increased substantially (from  $0.9 \pm 0.22 \mu\text{A}$  to  $4.2 \pm 0.45 \mu\text{A}$ ) following chloroform vapor annealing and even exceeded that of the as-prepared P3BT. As the cross-section of the P3BHT stripes before and after vapor annealing

- [1] a) J. Xu, J. Wang, M. Mitchell, P. Mukherjee, M. Jeffries-El, J. W. Petrich, Z. Q. Lin, *J. Am. Chem. Soc.* **2007**, *129*, 12828; b) Z. Q. Lin, *Chem. Eur. J.* **2008**, *14*, 6294.
- [2] Z. Bao, A. Dodabalapur, A. J. Lovinger, *Appl. Phys. Lett.* **1996**, *69*, 4108.
- [3] a) R. J. Kline, M. D. McGehee, M. F. Toney, *Nat. Mater.* **2006**, *5*, 222; b) R. J. Kline, M. D. McGehee, E. N. Kadnikova, J. Liu, J. M. J. Fréchet, *Adv. Mater.* **2003**, *15*, 1519; c) R. Zhang, B. Li, M. C. Iovu, M. Jeffries-El, G. Sauvé, J. Cooper, S. Jia, S. Tristram-Nagle, D. M. Smilgies, D. N. Lambeth, R. D. McCullough, T. Kowalewski, *J. Am. Chem. Soc.* **2006**, *128*, 3480; d) H. Sirringhaus, P. J. Brown, R. H. Friend, M. M. Nielsen, K. Bechgaard, B. M. W. Langeveld-Voss, A. J. H. Spiering, R. A. J. Janssen, E. W. Meijer, P. Herwig, D. M. de Leeuw, *Nature* **1999**, *401*, 685.
- [4] M. He, F. Qiu, Z. Lin, *J. Mater. Chem.* **2011**, *21*, 17039.
- [5] a) M. He, W. Han, J. Ge, Y. Yang, F. Qiu, Z. Lin, *Energy Environ. Sci.* **2011**, *4*, 2894; b) R. S. Loewe, S. M. Khersonsky, R. D. McCullough, *Adv. Mater.* **1999**, *11*, 250.
- [6] a) G. H. Lu, L. G. Li, X. N. Yang, *Adv. Mater.* **2007**, *19*, 3594; b) A. Salleo, R. J. Kline, D. M. DeLongchamp, M. L. Chabinyc, *Adv. Mater.* **2010**, *22*, 3812.

- [7] W. Han, Z. Lin, *Angew. Chem.* **2012**, *124*, 1566; *Angew. Chem. Int. Ed.* **2012**, *51*, 1534.
- [8] a) S. W. Hong, J. Xu, Z. Q. Lin, *Nano Lett.* **2006**, *6*, 2949; b) J. Xu, J. F. Xia, Z. Q. Lin, *Angew. Chem.* **2007**, *119*, 1892; *Angew. Chem. Int. Ed.* **2007**, *46*, 1860; c) M. Byun, R. L. Laskowski, M. He, F. Qiu, M. Jeffries-El, Z. Q. Lin, *Soft Matter* **2009**, *5*, 1583; d) J. Xu, J. F. Xia, S. W. Hong, Z. Q. Lin, F. Qiu, Y. L. Yang, *Phys. Rev. Lett.* **2006**, *96*, 066104; e) M. Byun, N. B. Bowden, Z. Lin, *Nano Lett.* **2010**, *10*, 3111; f) W. Han, M. Byun, B. Li, X. Pang, Z. Lin, *Angew. Chem.* **2012**, *124*, 12756; *Angew. Chem. Int. Ed.* **2012**, *51*, 12588.
- [9] M. Abkarian, J. Nunes, H. A. Stone, *J. Am. Chem. Soc.* **2004**, *126*, 5978.
- [10] S. W. Hong, J. Wang, Z. Q. Lin, *Angew. Chem.* **2009**, *121*, 8506; *Angew. Chem. Int. Ed.* **2009**, *48*, 8356.
- [11] a) M. He, L. Zhao, J. Wang, W. Han, Y. Yang, F. Qiu, Z. Lin, *ACS Nano* **2010**, *4*, 3241; b) L. Zhao, X. Pang, R. Adhikary, J. W. Petrich, M. Jeffries-El, Z. Lin, *Adv. Mater.* **2011**, *23*, 2844; c) L. Zhao, X. Pang, R. Adhikary, J. W. Petrich, Z. Lin, *Angew. Chem.* **2011**, *123*, 4044; *Angew. Chem. Int. Ed.* **2011**, *50*, 3958.
- [12] S. W. Hong, J. F. Xia, Z. Q. Lin, *Adv. Mater.* **2007**, *19*, 1413.
- [13] L. Robinson, J. Isaksson, N. D. Robinson, M. Berggren, *Surf. Sci.* **2006**, *600*, L148.
- [14] a) W. L. Ma, C. Y. Yang, X. Gong, K. Lee, A. J. Heeger, *Adv. Funct. Mater.* **2005**, *15*, 1617; b) V. D. Mihailetschi, H. X. Xie, B. de Boer, L. J. A. Koster, P. W. M. Blom, *Adv. Funct. Mater.* **2006**, *16*, 699.
- [15] a) G. Li, V. Shrotriya, J. S. Huang, Y. Yao, T. Moriarty, K. Emery, Y. Yang, *Nat. Mater.* **2005**, *4*, 864; b) H. Tang, G. Lu, L. Li, J. Li, Y. Wang, X. Yang, *J. Mater. Chem.* **2010**, *20*, 683; c) F. C. Chen, C. J. Ko, J. L. Wu, W. C. Chen, *Sol. Energy Mater. Sol. Cells* **2010**, *94*, 2426; d) V. Shrotriya, Y. Yao, G. Li, Y. Yang, *Appl. Phys. Lett.* **2006**, *89*, 063505.
- [16] H. H. Yang, S. W. LeFevre, C. Y. Ryu, Z. N. Bao, *Appl. Phys. Lett.* **2007**, *90*, 172116.
- [17] J. Ge, M. He, F. Qiu, Y. Yang, *Macromolecules* **2010**, *43*, 6422.
- [18] J. Ge, M. He, X. Yang, Z. Ye, X. Liu, F. Qiu, *J. Mater. Chem.* **2012**, *22*, 19213.
- [19] G. H. Lu, H. W. Tang, Y. A. Huan, S. J. Li, L. G. Li, Y. Z. Wang, X. N. Yang, *Adv. Funct. Mater.* **2010**, *20*, 1714.
- [20] a) A. J. Heeger, S. Kivelson, J. R. Schrieffer, W. P. Su, *Rev. Mod. Phys.* **1988**, *60*, 781; b) J. Roncali, *Chem. Rev.* **1992**, *92*, 711.